Optics & Laser Technology 43 (2011) 1054–1060

Contents lists available at ScienceDirect

Optics & Laser Technology

journal homepage: www.elsevier.com/locate/optlastec

Multi-mode opto-thermo-mechanical stretching system for determination of 3D refractive index along the axis of stretched and/or heated fibres

T.Z.N. Sokkar [a], M.M. El-Tonsy [a], M.A. El-Morsy [b], S.M. El-Khateep [a,*], M.I. Raslan [a]

[a] Physics Department, Faculty of Science, Mansoura University, Mansoura 35516, Egypt
[b] Physics Department, Demietta Faculty of Science, Mansoura University, New Demietta, Egypt

ARTICLE INFO

Article history:
Received 20 September 2010
Received in revised form
6 December 2010
Accepted 22 December 2010
Available online 3 March 2011

Keywords:
Isotactic polypropylene, (iPP)
Pluta polarising interference microscope and subfringe
Analysis technique

ABSTRACT

A multi-mode opto-thermo-mechanical stretching system was modified to study the changes in the 3D of optical and structural properties of stretched fibre along its axis. The structural deformation of isotactic Polypropylene, (iPP), fibres was studied at different draw ratios. The modified system coupled with Pluta polarising interference microscope was used to determine the variation of the birefringence in three dimensions during stretching process. Using this modified system, the multi-necking was detected. Subfringe analysis technique was used to determine the phase distribution of the obtained microinterferograms, which were given for illustration.

1. Introduction

Isotactic Polypropylene (iPP) is extensively used in industry to manufacture bottles, films, and fibres. The heat and draw deformation behaviour of iPP is of significant practical importance in terms of both its product performances and manufacturing processes. The mechanical properties and morphology of the product are strongly affected not only by its molecular characteristics such as the molecular weight (MW) and molecular weight distribution (MWD) [1–4] but also by its processing conditions such as the drawing temperature, the drawing ratio, the strain rate and the cooling rate after drawing [5–7]. Finally, knowledge of the structural deformation during drawing process is essential to predict the product performance.

The refractive indices and birefringence of polymeric fibres are important because they are related to some internal structural properties. Previous studies on the polymer used in textile fibre show different values of refractive indices when they are measured parallel and perpendicular to the fibre axis. This difference depends on the orientation of the molecular chains [8].

Drawing (stress–strain) is an important operation that improves the textile characteristics of man-made fibres. Undrawn synthetic fibres are almost isotropic in their physical properties. They exhibit low tenacity, low modulus of elasticity, high plastic deformability, etc. To turn them into useful fibres for textile and industrial use they must be drawn. This results in stronger, more birefringent fibres that are highly anisotropic. Besides the various techniques such as IR, UV, NMR, and X-ray, the microinterferometric measurements of refractive indices and birefringence still are valuable tools for the characterisation of these fibres. For instance, the value of the birefringence of undrawn and drawn fibres is a useful parameter for monitoring the drawing process. To optimise any technical drawing process, one should know the relationships between undrawn material structure and the structural properties of the drawn fibres. One of these useful relationships is the stress–strain curve of undrawn fibres, which provides the yield stress, the tensile modulus, and the stability of deformation for these fibres [9,10]. Drawing is one of the most common methods for changing the physical properties of a polymeric material to strengthen it during processing. This drawing orients its chains and super molecular structures. If the polymer is an amorphous one with molecules of regular structures, it may even crystallise. The degree of axial orientation, often characterised by optical birefringence, increases with increasing draw ratio. The degree of orientation effectively produced in the drawing process depends on the draw ratio, drawing conditions, and composition of the fibre [11].

The cold drawing of a semi-crystalline polymeric fibre induces a deep structural rearrangement as the initial morphology is transformed into the final fibrous organisation. Since the transformation is irreversible and occurs under non-equilibrium thermodynamic conditions, the fibre obtained is a system in a metastable state [12]. Studying the deformation mechanisms during uni-axial drawing of fibres is a useful process to

* Corresponding author. Tel.: +20 0502246104; fax: +20 0502246781.
E-mail address: samar_elkhateep@mans.edu.eg (S.M. El-Khateep).

0030-3992/$ - see front matter © 2011 Elsevier Ltd. All rights reserved.
doi:10.1016/j.optlastec.2010.12.015

characterize the opto-mechanical properties of textile fibres made from polymers materials [13]. In the case of semi-crystalline polymers such as iPP fibres, yielding and cold drawing contain two types of non-uniform deformation processes: the first one is the initiation of local necking and the other is the propagation of neck shoulders along the sample. Both types result from the local instability of deformation but they are different in behaviour [14].

Orientation in polymers can be produced by several processes such as hot stretching or by cold drawing. The drawing process gives rise to preferred orientation of the molecular chain axis. The degree of orientation could vary significantly from one fibre to another depending on the fibre history during manufacture and subsequent processing operations. The phenomenon of cold drawing is common to both amorphous and semi-crystalline polymers [15,16].When some polymers are drawn at low draw ratios, they deform and show a narrowing of the thickness (called necking) [17]. Necking is a smooth jump in cross-sectional area of long and thin bars propagating with a constant speed. This necking phenomenon usually occurs when a homogeneous solid polymeric bar (fibre or film) is stretched uni-axially [18]. In this case, this polymer fibre is not deformed homogeneously. Instead of this, two almost uniform sections occur in the sample: one is nearly equal to its initial thickness and the other is considerably thinner in the cross-sectional dimensions. These sections are joined by a relatively short transition (necking) zone that propagates with a constant speed along the fibre as a stepwise wave in the direction of the fibre's thick end. They considered that the formation of these neck zones is due to microscopic inhomogeneities. This is attributed to the orientation of polymer molecules. Also it was shown that there is a sudden structural transformation in the neck shoulder during solid-state drawing. El-Dessouky [19] characterised the necking phenomenon of iPP fibres using the Pluta polarising interference microscope in its substractive position. The necking phenomenon can be avoided by controlling the rate of drawing of the fibre. It is recommended to stretch the iPP fibres with slow (step) drawing to avoid the necking deformation [20].

Several works were dedicated to the online investigation of stretched fibres. Sokkar et al. [21] previously presented a novel video opto-mechanical device that studied the effect of stretching speed on the optical and structural properties of fibres during the dynamic stretching process. This work carried for the segment of the tested fibre shown in the microscope's field of view.

The aim of this work is to present an online system for studying the stretching process along the fibre axis, which is useful to detect the presence of multi-necking regions at different positions along the fibre.

2. Theoretical considerations

2.1. Birefringence profile

The birefringence profile, $\Delta n = n^{||} - n^{\perp}$ of two-beam fringes crossing a cylindrical fibre having multilayer structure was obtained. Each term of the equation represents the contributions of each layer constituting the multilayer fibre. This treatment considers the transverse refraction. It leads to the expression [22]:

$$\Delta n_Q = \left[\frac{1}{R-(Q-1)a}\right]\left[\frac{\lambda \Delta Z_Q}{2b} - a\sum_{j=1}^{j=Q-1}\Delta n_j\right] \tag{1}$$

where Δn is the birefringence, Q is the layer number, j is the integer number ($j=1$: $Q-1$), λ is the wavelength of monochromatic light used, Z is the fringe shift, b is the interfringe spacing, R is the radius of the fibre, and a is the layer thickness.

2.2. Orientation function

To show the effect of stretching process on the structure of fibres, the orientation function may be calculated. The Hermans orientation function $F(\theta)$ is probably the quantity most frequently used to characterize the orientation. For a drawn fibre where the molecules are considered to be aligned along the draw direction but only randomly arranged in the transverse section, The Herman's orientation factor $F(\theta)$ is related to the birefringence Δn by the following equation [23]:

$$F(\theta) = \frac{\Delta n_Q}{\Delta n_{\max}} \tag{2}$$

where $\Delta n_{\max}$ is the intrinsic maximum birefringence equal to 0.03 for iPP fibres [24].

2.3. Fringe analysis using subfringe integration technique

The microinterferograms were analysed using the subfringe integration technique [25]. The main idea of subfringe integration method is that the period of the sinusoidal signal, given by Eq. (3), is divided into at least three or more buckets and integrates each bucket. Four integrating buckets (cf. [25]) in the spatial domain are used.

$$I(x,y) = a(x) + b(x)\left[\cos\frac{2\pi}{\lambda}x + \varphi(x,y))\right] \tag{3}$$

where, $a(x)$ represents the background illumination of the intensity distribution $I(x)$ and $b(x)$ describes the amplitude of the corresponding interference fringe.

The four-intensity integration bucket over a finite space can be described as

$$\begin{aligned} I &= \int_{-(T/8)}^{T/8} I(x)dx + \int_{T/8}^{3T/8} I(x)dx + \int_{3T/8}^{5T/8} I(x)dx + \int_{5T/8}^{7T/8} I(x)dx \\ &= I_1 + I_2 + I_3 + I_4 \end{aligned} \tag{4}$$

In this case, the phase φ is given by

$$\varphi = \tan^1\left(\frac{I_4 - I_2}{I_1 - I_3}\right) \tag{5}$$

According to the limits of integration we need to shift the origin of the signal by $T/8$.

But for more accuracy, they changed the limits of integration to (0, $T/4$), ($T/4$, $T/2$), ($T/2$, $3T/4$), and ($3T/4$, T).

In this case we do not need to shift the origin of the signal. Eq. (4) becomes

$$\begin{aligned} I &= \int_{0}^{T/4} I(x)dx + \int_{T/4}^{T/2} I(x)dx + \int_{T/2}^{3T/4} I(x)dx + \int_{3T/4}^{T} I(x)dx \\ &= I_1 + I_2 + I_3 + I_4 \end{aligned} \tag{6}$$

where

$$\begin{aligned} I_1 &= A + B[\cos\varphi - \sin\varphi] \\ I_2 &= A + B[-\cos\varphi - \sin\varphi] \\ I_3 &= A + B[-\cos\varphi + \sin\varphi] \\ I_4 &= A + B[\cos\varphi + \sin\varphi] \end{aligned} \tag{7}$$

and

$$A = \frac{T}{4}a(x), \quad B = \frac{T}{2\pi}b(x)$$

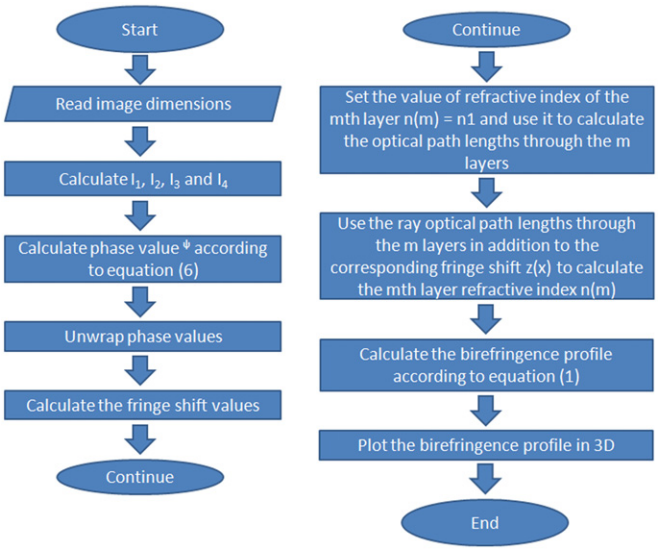

Fig. 1. Flowchart of the used software for fringe analysis.

The phase is giving by applying the equation

$$\varphi = \tan^{-1}\left(\frac{(I_1+I_2)-(I_3+I_4)}{2(I_2-I_1)}\right) \tag{8}$$

Fig. 1 shows the flowchart of the designed software used in determining the birefringence profile in three dimensions. The measuring accuracy of the birefringence profile using this model is (0.003–0.001) [26,27].

3. Experimental technique

3.1. Multi-mode opto-thermo-mechanical stretching system

This system is designed to be coupled with the well known Pluta polarising interference microscope. It is a programmable system, able to achieve different detections through a software controlling process. Fig. 2 shows the main construction of this system. A long piece of continuous fibre is wound around one of the cylinders M_1 or M_2, the free end of this fibre is passed through holes in the magnetic clamps C_1C_2 and then stuck on the surface of the second cylinder. The fibre will pass touching the surface of a glass slide S, which is rested above a flat thin heater H. The magnetic clamps C_1C_2 can now be pushed forward and backward to locate the fibre, nearly, at the centre of the field of view by the microscope. The microscope can now be adjusted normally to display the duplicated or non-duplicated image after introducing a suitable immersion fluid on the fibre, before running start of the video camera, then the action mode of the opto-mechanical system should be configured from the stepper motors running software. Four action modes can be initialised by this system, which are:

3.1.1. Longitudinal testing mode

This mode of action allows capturing a video clip showing interference fringe shifts across thousands of the fibre sections along its axis, which in turn helps to determine changes in the refractive index profile along the fibre axis.

3.1.1.1. Software configuration. To initialise this mode, simply, put the two stepper motors M_1 and M_2 to the same rotational speed and in the same direction. So, the length of fibre that unwound from the first cylinder will be exactly wound on the other cylinder

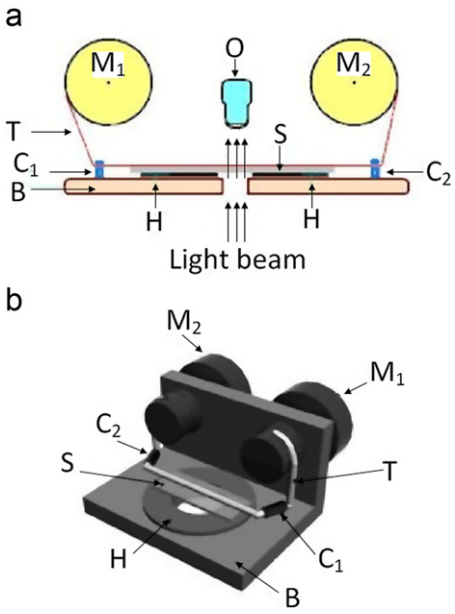

Fig. 2. (A) Schematic diagram of multi-mode opto-thermo-mechanical stretching system, where, M_1 and M_2 are two symmetrical cylinders axially fixed to two identical stepper motors, T is the fibre under test, S is a flat glass slid, B is a metallic base, C_1, C_2 are the magnetic clamps, H is the thin flat heater rated at 20 W, 110 V, coupled with electronic temperature controller, and O is the objective lens of a Pluta polarising interference microscope provided with a video camera of fixed frame rate. (B) The 3D view.

without any stretching. During the transfer of certain fibre segment from the first cylinder to the second, it passes just under the objective lens of the microscope and the video camera records all fringe shifts that belong to this segment.

3.1.1.2. Calculations. The main task in this mode is to find the match between every frame in the video clip and the location of the fibre section that belongs to this frame. Let r be the radius of the cylinder that is rotating by M_1 and f be the rotational speed of motor M_2 in step/s and m be the number of steps per one complete revolution, then the length L of fibre that unwound per second is

$$L = \frac{2\pi rf}{m} = 2\pi r\left(\frac{f}{m}\right) \tag{9}$$

If (F) is the frame rate of recording the clip, then two successive frames show interferograms for two fibre sections at distance X from each other, where:

$$X = \frac{L}{F} = \frac{2\pi rf}{mF} \tag{10}$$

with maximum expected error of $\pm 10^{-2}$ millimetre.

3.1.1.3. Cases of use. This mode of operation is useful for studying the type, amount, and sequence of industrial defects during the mass production of long continuous filaments of polymeric fibres.

3.1.2. Dynamic stretching mode

When a fibre undergoes a mechanical stretching, it suffers from some structural variations. These variations are detectable by many techniques, but the detection is carried out after the end of stretching process. This means that the detected variations are the net values after relaxation of most variations. The dynamic stretching mode of test by the current system allows the detection of real variations online, on both qualitative and quantitative levels.

3.1.2.1. Software configuration. To initialise this mode select different rotational speeds for the wheels M_1 and M_2 but let M_1 and M_2 to rotate in same direction. If the whole fibre sample was wound on M_1 then M_2 should rotate faster than M_1, so that stretching takes place continuously. Let f_1 and f_2 be the rotational speeds of M_1 and M_2, respectively, in the unit of step/s, then the stretching process causes drawing of the fibre with draw ratio of $Dr=f_2/f_1$; this ratio holds as long as f_2/f_1 remains unchanged.

3.1.2.2. Calculations. This ratio f_2/f_1 determines the drawing ratio of the fibre during the stretching process, but the stretching speed is another important factor that affects the response of fibre structure.

In order to calculate this speed, the unit of measuring this speed should be defined initially. The quantity (f_2-f_1) gives the stretching speed in unit of step/s. To convert this unit to length/s, it can be done easily by replacing (f) in Eq. (9) by (f_2-f_1), so

$$\text{Stretching speed } V_s=\frac{2\pi r(f_2-f_1)}{m} \tag{11}$$

In this formula it was assumed that both motors M_1 and M_2 are characterised by the same number m of steps per complete revolution.

If this assumption does not hold good, then

$$V_s=2\pi r\left(\left(\frac{f_2}{m_2}\right)-\left(\frac{f_1}{m_1}\right)\right) \tag{12}$$

where m_1 and m_2 are numbers of steps per revolution of M_1 and M_2, respectively. It is clear from Eqs. (11) and (12) that V_s is constant as long as f_2 and f_1 remain unchanged.

3.1.2.3. Cases of use. This mode is useful for studying industrial defects during manufacturing of continuous long fibres, especially those defects that cannot be detected by static or stationary tests, for example, mutual adhesion at boundaries of multi-layered fibres.

3.1.3. One point stretching mode

When an undrawn fibre undergoes a continuous stretching until it breaks, it suffers from thinning, necking, and breaking. To detect and characterize these stages quantitatively and qualitatively on the atomic or molecular levels, it is essential to measure the change of refractive indices and birefringence at certain fibre sections during stretching.

3.1.3.1. Software configuration. To initialise this mode of operation, let both wheels that are attached to motors M_1 and M_2 rotate with the same speed but in opposite directions. This condition forces the fibre to be stretched without any translation and hence the polarising interference microscope and camera record change in a certain fibre section due to continuous growing of strain at fixed rate.

3.1.3.2. Calculations. The important parameter, involved in this mode is the rate of elongation (Re), which may defined as the increase in fibre length per unit time at constant force, then the measuring unit of (Re) is m/s. It is clear that Re has units of velocity; therefore (Re) may be called elongation speed. Eq. (11) can be applied to the recent mode by taking $|f_1|=|f_2|=f_0$ and by considering the direction of rotation, then $f_2=f_0$ and $f_1=-f_0$, then Eq. (11) gives

$$\text{Re}=\frac{2\pi r(f_0-(-f_0))}{m}=4\pi r\left(\frac{f_0}{m}\right) \tag{13}$$

Hence, after t seconds from the start of stretching the image captured for the specified fibre section represents the state of this section at total elongation of $4\pi r f_0 t/m$, with maximum expected error of $\pm 10^{-2}$ mm.

3.1.3.3. Cases of use. Detection of opto-mechanical response of a fibre may provide good information about both mechanical and structural properties of the fibre material. If a fibre was free from any industrial defects, then the one point stretching mode may be useful for the determination of average mechanical and structural properties of fibre's material by testing several sections separately.

3.1.4. Thermo-mechanical mode

This mode of operation helps to detect the structural variations of fibres at elevated temperature; also it detects the one point stretching behaviour, as in mode III, but at higher temperature. This thermo-mechanical mode will be given in further future work.

4. Experimental results and discussion

In this paper, the first and second modes are applied. The used sample is iPP fibre. This fibre is as-spun undrawn monofilement of isotactic polypropylene textile fibres manufactured at spinneret, and take up speed=150 m/s with temperature zone equal to 350–450 °C. The sample is immersed in a suitable liquid with a refractive index $n_L=1.500$ at room temperature $T=25$ °C. The wavelength of monochromatic light used is 546.1 nm. The obtained video film is captured and separated into frames. In the stretching process, two stepper motors with resolution 200 steps/revolution were automatically controlled using a suitable software. This gives more accurate strain measurements during the drawing process of iPP fibres. The stepper motors apply stress on the stretching sample at constant rate. After the stretching process, the two motors rotate with the same speed and direction allowing us to scan the stretched sample longitudinally to investigate the necking phenomenon formed during the stretched process. This process was carried out at room temperature. Further modifcations were made to the opto-mechanical system to be suitable for investigations carried out at higher temperatures, which will be introduced in future work.

The sample is fixed from its ends on the two motors (M_1, M_2) and put in the focus of the objective lens of the Pluta polarising interference microscope. M_1 and M_2 are rotated at different speeds so that, the sample is drawn to a certain draw ratio. During the stretched process, necking phenomenon is observed at different positions on the fibre axis. Furthermore under increased loading, stable propagation of the necks takes place. Then the two motors are set to rotate at the same speed ($v=4$ step/s) to scan over the length of the stretched sample. Microinterferograms are recorded continuously for the scanned sample, which helps in detecting the necking at different places, as well as, different structural variations.

Microinterferograms are captured via a CCD camera connected to a computerised unit. Fig. 3A–F shows the interferograms of non-duplicated position (birefringence) for iPP fibres at different values of draw ratios (1.5, 2, 2.5, 3, and 3.5). Besides studying the optical properties, the variation of the cross-section of the fibre can be observed from the shifted fringes due to the presence of the fibre sample. This denotes the positions where the necking regions are found, as it is clear from Fig. 3B and F, where the necking is observed at the centre of the field.

The contours of the obtained interference patterns are determined using our designed software. It is clear from Fig. 3G–L that, there are observed variations in the shift of the contour lines, denoting changes in the value of the molecular orientation.

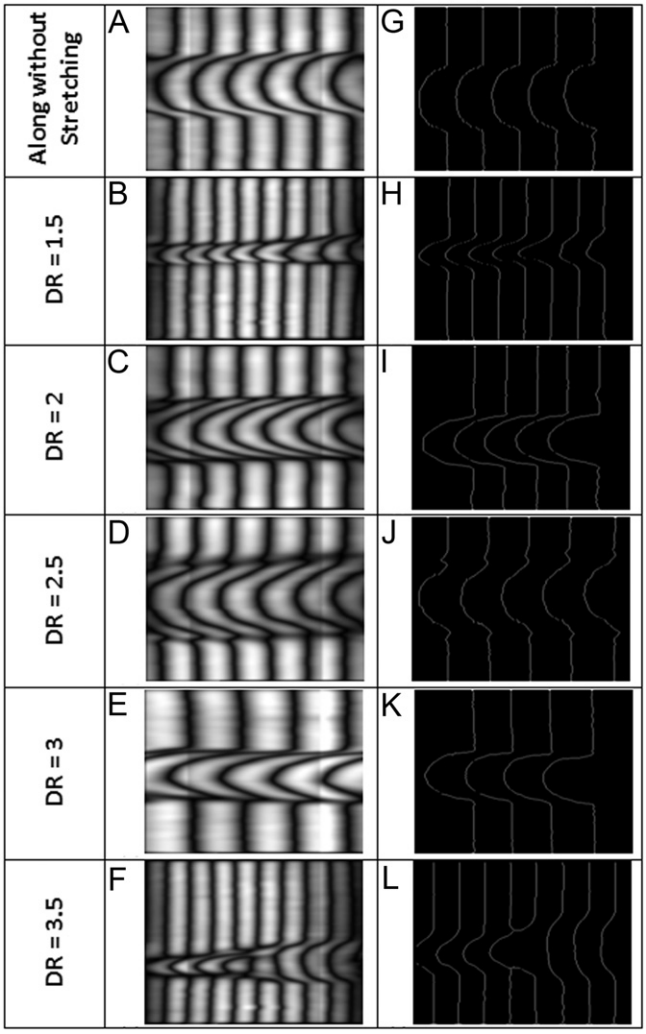

Fig. 3. (A–F) Microinterferograms of the two-beam polarising interference polarising microscope of iPP fibre at different draw ratios. (G–L) The obtained contour lines.

Fig. 3G demonstrates the sample that was not stretched, and we found there is no change in the value of the birefringence along the sample. On the other hand, Fig. 3H and L shows the changes of the fringe shifts along iPP sample stretched at different draw ratios from which different variations of the optical and structural properties are observed. The obtained contours of the fringes maxima allow us to study the necking phenomenon detected at different positions along the fibre sample.

The birefringence is determined along the sample of iPP fibres at different draw ratios. Fig. 4 shows the birefringence along as-spun sample of iPP fibres, while Figs. 5–9 show the 3D birefringence along the stretched iPP sample at different draw ratios. Necking regions are observed at different positions as it is clear from the figures. Also, these figures denote the distribution of the molecular orientation at different positions along the fibre's material. Fig. 10 shows the variation in the shape of the fibre obtained from the captured microinterferograms, this helps in recognising different parts of structural changes along the fibre, e.g. necking. From the obtained Fig. 10a–f, this technique is helpful in imaging different shape deformations observed for the stretched iPP fibres. In Fig. 5 it can be observed that, different necking positions are observed when the sample stretches to the draw ratio (DR=1.5). This also appears in Figs. 6–9. Using Eq. (2) and designed software the 3D orientation function along the stretched iPP sample at draw ratio (DR=3.5) is calculated. This 3D molecular orientation function gives the same feature of 3D birefringence shown in Fig. 9. Upon stretching, the molecular

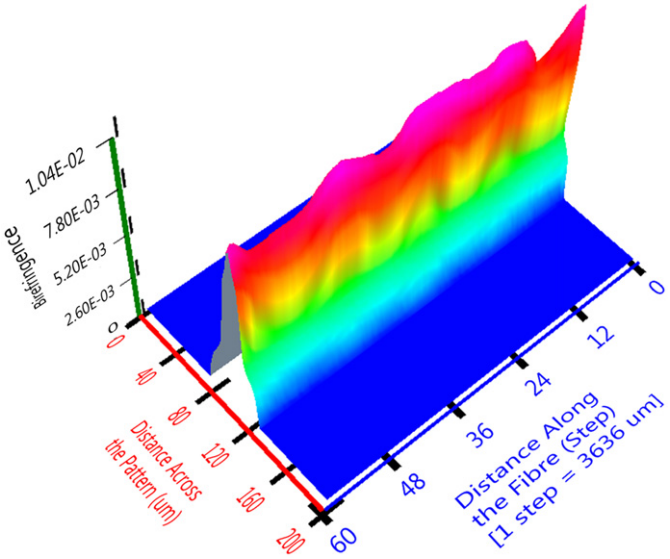

Fig. 4. 3D birefringence along iPP fibre without stretching.

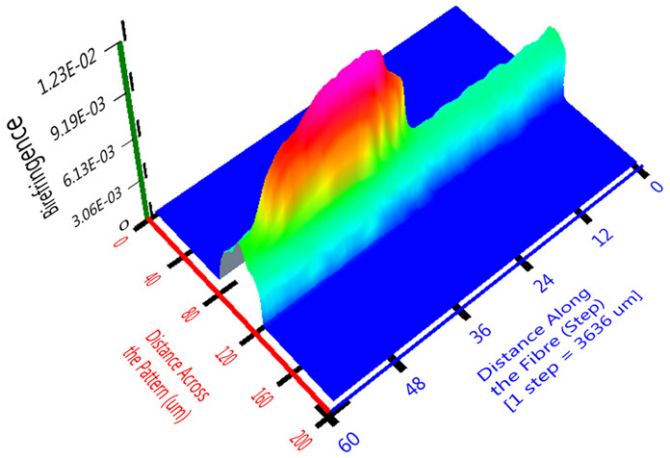

Fig. 5. 3D birefringence at DR=1.5.

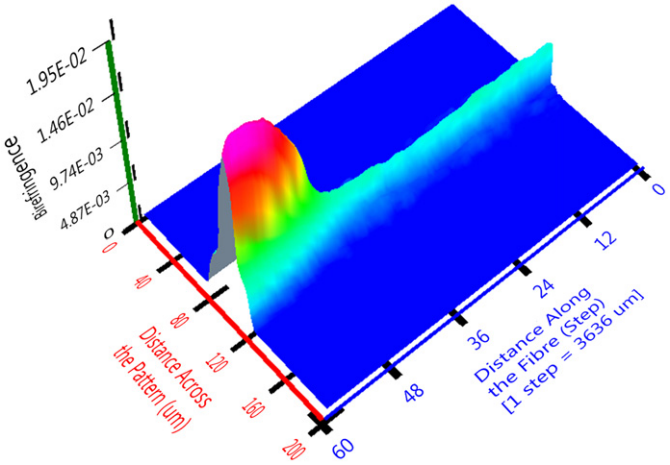

Fig. 6. 3D birefringence at DR=2.

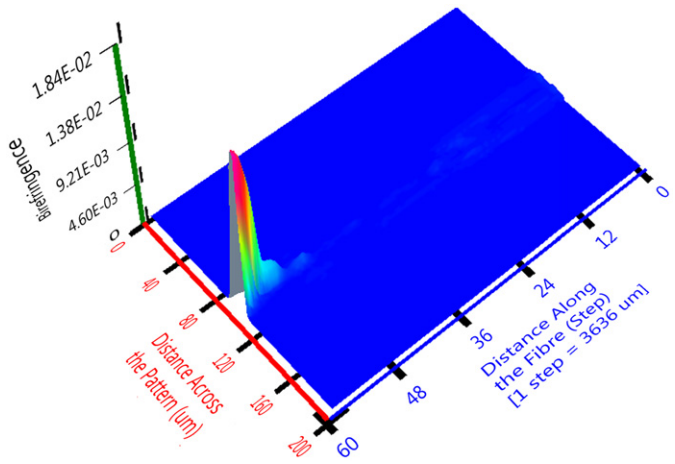

Fig. 7. 3D birefringence at DR=2.5.

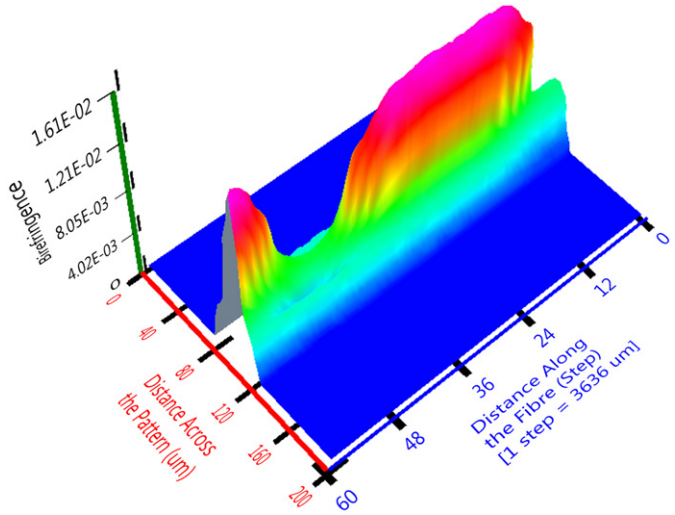

Fig. 8. 3D birefringence at DR=3.

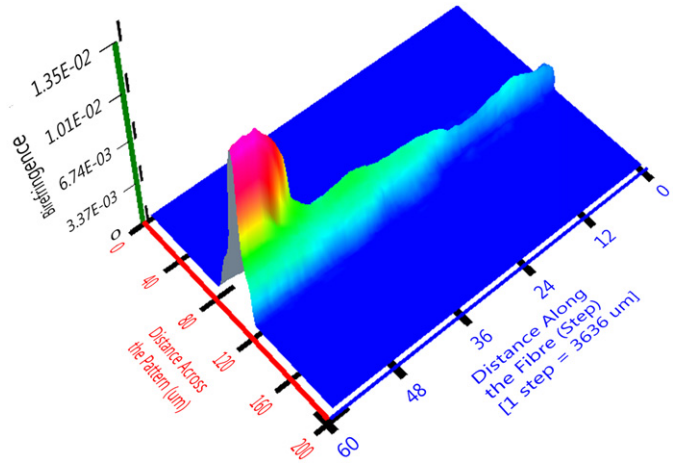

Fig. 9. 3D birefringence at DR=3.5.

orientation increases showing molecular orientation to be higher at the necking regions than any other regions. This implies that, the necking regions observed during stretching iPP fibres are smooth transition zones between the thick and thin parts of iPP fibres. The regions before necking (thick regions) are less oriented than the regions after necking (thin regions) while the orientation at the necking regions is intermediate between them. This is attributed to the fact that, drawing processes induce more molecular orientation for the stretched samples of iPP fibres.

Several facts are observed from the behaviour of the birefringence values in three dimensions along the fibre. Fig. 4 shows the distribution of the birefringence along as-spun sample of iPP. From this figure, it is observed that, there is no appreciable variation in the birefringence along the fibre sample; on the other hand, the maximum value of the birefringence is observed at the innermost layers. Also there is a gradual decrease in the birefringence when going towards the outer layers. For the drawn iPP samples, in Fig. 5, values of the distances along the fibre axis were given in steps, each step equal to 3636 μm. The necking region was observed in the region (10–20) steps, which is equivalent to (36,360–72,720) μm. It is detected as an elevation in the values of the birefringence and narrowing in the cross-section. It can be viewed more clearly from Fig. 10b, which is a 3D shape view of Fig. 5, which clearly identifies the necking region. Also, this is observed in Figs. 6 and 7 where a single necking is observed along the stretched sample. On the other hand, Fig. 8 shows a multi-necking phenomenon detected along the stretched iPP sample to draw ratio (DR=3). This figure shows two necking regions, observed elevations in the values of the refractive indices, and thinner cross-section. The fibre shape shown in Fig. 10e clearly shows the multi-necking phenomenon observed at (DR=3). Also, stretching iPP fibres to draw ratio (DR=3.5) shows a multi-necking phenomenon observed as four necking regions along the stretched sample. Grady and Benson [28] observed that the number of necking is an increasing function of the draw ratio. This observation confirms our experimental results given from Figs. 4–10 that show that the number of necking increases with increasing draw ratio. Also Altynove et al. [29] observed the same results for the multiple necking.

Necking formation is controlled by different factors that were discussed by different authors [30]. Mainly stretching speed and final draw ratio are the main parameters controlling the necking formation. From observations, higher draw ratios cause the formation of multi-necking more than lower draw ratios. This fact is clear from the calculation of the fibre shape based on the experimentally obtained microinterferograms as shown in Fig. 10.

5. Conclusion

A multi-mode opto-thermo-mechanical stretching system attached with a Pluta polarising interference microscope is designed. The advantage of this device is the determination of the refractive indices and birefringence of fibres for each draw ratio during the online stretching process. Also the designed system allowed us to investigate the variation of the optical properties along the stretched iPP fibres. From the measured birefringence we calculated the changes of the molecular orientation function at different positions of the stretched sample. This investigation allowed us to detect the presence of multi-necking regions at different positions along the fibre. Also, the measured birefringence and the calculated orientation function in 3D allowed us to study the necking phenomenon in more detail.

Acknowledgment

We would like to express our deep thanks to prof. Dr. A.A. Hamza, for his useful discussions and lending many facilities.

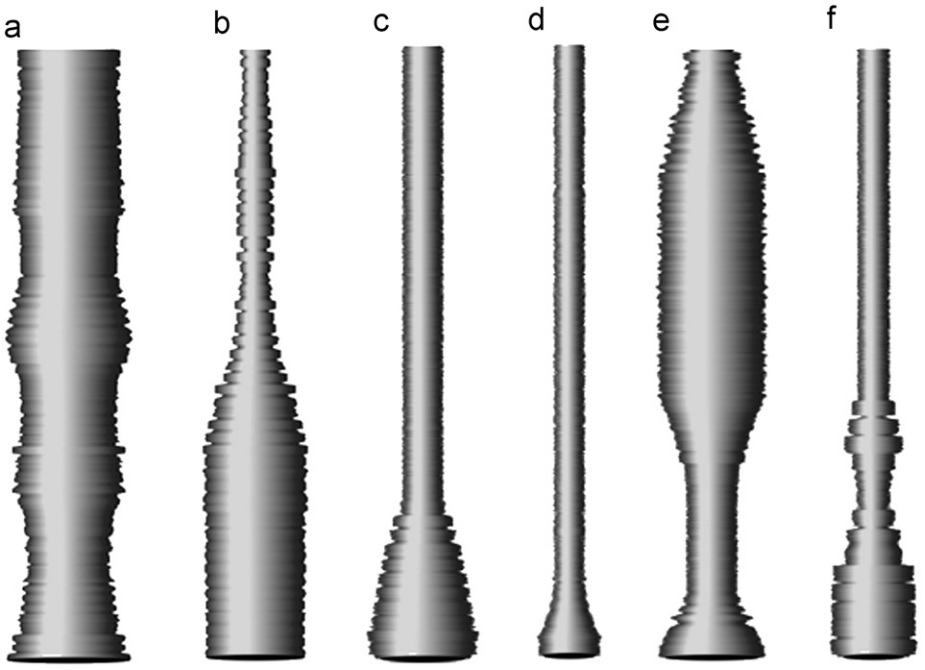

Fig. 10. 3D shape of iPP fibre, (a) along iPP fibre without stretching, (b) at DR=1.5, (c) at DR=2, (d) at DR=2.5, (e) at DR=3, and (f) at DR=3.5.

References

[1] Brown N, Ward IM. The influence of morphology and molecular weight on ductile-brittle transitions in linear polyethylene. J Mater Sci 1983;18:1405.
[2] Chu JN, Schultz JM. Surface properties and adhesion mechanisms of graft polypropylenes. J Mater Sci 1989;24:4538.
[3] Flood JE, Nulf SA. How molecular weight distribution and drawing temperature affect polypropylene physical properties and morphology. Polym Eng Sci 1990;30:1504.
[4] Fujiyama M, Kitajima Y, Inata H. Rheological properties of polypropylenes with different molecular weight distribution characteristics. J Appl Polym Sci 2002;84:2128.
[5] Karacan I, Taraiya AK, Bower DI, Ward IM. Characterization of orientation of one-way and two-way drawn isotactic polypropylene films. Polymer 1993; 34:2691.
[6] Alberola N, Fugier M, Petit D, Fillon B. Tensile mechanical behavior of quenched and annealed isotactic PP films. J Mater Sci 1995;30:860.
[7] Stefan R, Ludovic C, Helmut M, Klaus S, Johannes S. Uniaxial deformation behavior of different polypropylene cast films at temperatures near the melting point. Rheol Acta 2002;41:332.
[8] Shams-Eldin MA, Studies on Some Structural Properties of Textile Fibers, MSc, Mansoura Univ., Egypt, 1997.
[9] Gaur AH, De Vries H. On the refractive indexes and birefringence of nylon 6 yarns as a function of draw ratio and strain. J Polym Sci 1975;13:835.
[10] Zbigniew KW. Formation of Synthetic Fibers. New York: Gordon and Breuch Science Publishers; 1977. Chapter 7.
[11] Tager A. Physical Chemistry of Polymers. Moscow: MIR; 1978.
[12] de Candia F, Russo R, Tidjani A, Vittoria V, Peterlin A. Aging phenomena in isotactic polypropylene drawn at different temperatures. J Plym Sci B: Polym Phys 1897;1988:26.
[13] Mabrouk MA. Two-beam interference detection of the changes in fibre structural parameters during low drawing process. Polym Test 2002;21:897.
[14] Kontou E, Farasoglou P. Determination of the true stress–strain behavior of polypropylene. J Mater Sci 1998;33:147.
[15] Andrew JM, Ward IM. The cold-drawing of high density polyethylene. J Mater Sci 1970:5.
[16] Ajji A, Cole KC, Dumouline MM, Ward IM. Orientation of amorphous poly(ethylene terephthalate) by tensile drawing, roll-drawing, and die-drawing. Polym Eng Sci 1801;1997:37.
[17] Sova M, Raab M, Sližová M. Polypropylene composite materials oriented by solid-state drawing: low-temperature impact behavior. J Mater Sci 1993;28: 6516.
[18] Leonov AI. A theory of necking in semi-crystalline polymers. J Rheol 1990; 34:155.
[19] El-Dessouky HM. Birefringent characterization of necking phenomena along cold-drawn polypropylene fibres; I-offline drawing. J Appl Polym Sci 2007; 105:757.
[20] Hamza AA, Belal AE, Sokkar TZN, El-Dessouky HM, Yassien KM. Detection of necking deformation along polypropylene fibres axis at low draw ratios using multiple-beam microinterferometry. Opt Laser Technol 2007;39: 681–9.
[21] Sokkar TZN, El-Tonsy MM, El-Bakary MA, El-Morsy MA, Ali AM. A novel video opto-mechanical (VOM) device for studying the effect of stretchingspeed on the optical and structural properties of fibres. Opt Laser Technol. 2008. doi:10.1016.
[22] Sokkar TZN, El-Dessouky HM, Shams-Eldin MA, El-Morsy MA. Automatic fringe analysis of two-beam interference patterns for measurement of refractive index and birefringence profiles of fibres. Opt Lasers Eng 2007;45: 431–41.
[23] Hermans PH. Contribution to the Physics of Cellulose Fibres. 1949. [Ref. Gedde UPW, Polymer Physics, Chapman Hall: London, (1995),194].
[24] El-Dessouky HM, Lawrence CA, Voice AM, Lewis ELV, Ward IM. An interferometric prediction of the intrinsic optical properties for cold-drawn iPP, PTFE and PVDF fibres. J Opt A: Pure Appl Opt 2007;9:1041–7.
[25] El-Morsy MA, Harada K, Itoh M, Yatagai T. A subfringe integration method for multiple-beam Fizeau fringe analysis. Opt Laser Technol 2003;35:225.
[26] Pluta M. A double refracting interference microscope with continuously variable amount and direction of wavefront shear. J Mod Opt 1971:661–7518 1971:661–75.
[27] Pluta M. Interference microscopy of polymer fibres. J Microsc 1972;96:309.
[28] Grady DE, Benson DA. Fragmentation of metal rings by electromagnetic loading. Exp Mech 1983;12:393–400.
[29] Altynove M, Hu X, Daehn GS. Increased ductility in high velocity electromagnetic ring expansion. Mteall Trans A 1996;27:1837–44.
[30] Hamza AA, Sokkar TZN, El-Bakary MA, Ali AM. On line interferometric investigation of the neck propagation phenomena of stretched polypropylene fibre. Opt Laser Technol 2010;42:703–9.